The added value of satellite observations of methane for understanding the contemporary methane budget

PHILOSOPHICAL TRANSACTIONS A

rsta.royalsocietypublishing.org

Research

Article submitted to journal

Subject Areas:
xxxxx, xxxxx, xxxx

Keywords:
xxxx, xxxx, xxxx

Author for correspondence:
Paul I. Palmer
e-mail: paul.palmer@ed.ac.uk

The added value of satellite observations of methane for understanding the contemporary methane budget

Paul I. Palmer[1,2,†], Liang Feng[1,2,†], Mark F. Lunt[1,†], Robert J. Parker[3,4], Hartmut Bösch[3,4], Xin Lan[5], Alba Lorente[6], Tobias Borsdorff[6]

[1]University of Edinburgh, Edinburgh, UK
[2]National Centre for Earth Observation, University of Edinburgh, Edinburgh, UK
[3]University of Leicester, Leicester, UK
[4]National Centre for Earth Observation, University of Leicester, Leicester, UK
[5]NOAA Global Monitoring Laboratory, Boulder CO, USA
[6]SRON Netherlands Institute for Space Research, Utrecht, The Netherlands
[†]Authors contributed equally.

Sparse surface observations have recorded large and incompletely understood changes to atmospheric methane (CH_4) this century. These data are invaluable for contextualizing recent atmospheric variations to those reported for previous decades, but their ability to reveal the responsible surface sources and sinks is limited by their geographical distribution that is biased to northern midlatitudes. Earth-orbiting satellites designed specifically to measure CH_4 columns have been available since 2009 with the launch of the Japanese Greenhouse gases Observing SATellite (GOSAT). We assess the added value of GOSAT to data collected by the US National Oceanic and Atmospheric Administration (NOAA), which have been the lynchpin for knowledge about atmospheric CH_4 since the 1980s. To achieve that we use the GEOS-Chem atmospheric chemistry transport and an ensemble Kalman Filter inverse method to infer *a posteriori* flux estimates from the NOAA and GOSAT data using common *a priori* emission inventories. We find the main benefit of the satellite data is from its additional coverage over the tropics where we report large increases since the 2014/2016 El Niño, driven by biomass burning, biogenic emissions and energy production. We use data from the newest operational satellite instrument, the TROPospheric Monitoring Instrument (TROPOMI), to show how better spatial coverage and finer spatially resolved measurements allow us to quantify previously unattainable diffuse sources of CH_4 thereby opening up a new research frontier.

THE ROYAL SOCIETY PUBLISHING

1. Introduction

Atmospheric methane (CH_4) absorbs and emits radiation at infrared wavelengths and therefore plays a role in determining Earth's radiative balance. It has a higher global warming potential than CO_2; after carbon monoxide it is the principal sink of the hydroxyl radical (OH), which is the major oxidant in the global troposphere; and contributes to the production of tropospheric ozone, another important greenhouse gas. Consequently, it is an ideal target for rapid reductions to make substantive progress towards meeting the aims of the Paris Agreement [40,41]. For all of these reasons it is a science priority to address our inability to attribute definitively recent and large changes in the global mass of atmospheric CH_4 since the turn of the century [39,40,57]. In this study, we compare what we understand about recent changes (2010–2019) in global and regional CH_4 emissions from ground-based data and from satellite column retrievals of CH_4 at short-wave infrared (SWIR) wavelengths.

Observed changes in atmospheric CH_4 are determined by surface emissions and by surface and atmospheric sinks [59]. The largest natural source is emissions from wetlands, with smaller natural emissions from freshwaters, onshore and offshore geological sources, wild animals, termites, permafrost soils, and open and coastal ocean. Anthropogenic emissions are dominated by agriculture, including enteric fermentation from ruminants, manure management, and rice cultivation, and by waste management that includes the microbial decomposition of organic material in landfills. Emissions from fossil fuels are approximately half to two thirds of those from agriculture and waste [59] and include coal mining, the oil and gas industry, and transport. Combustion of biomass and biofuel is also a significant source of CH_4. The dominant loss process for CH_4 is oxidation by tropospheric OH, with small losses from stratospheric loss, reaction with chlorine, and uptake from soils. The resulting steady-state atmospheric lifetime of CH_4 is $\simeq$9 years [55]. The perturbation lifetime of CH_4, which accounts for atmospheric chemistry relaxation times and is more relevant for climate impacts of emission reductions is approximately 12 years [38].

After decades of steady growth in the 20th century, the atmospheric growth of atmospheric CH_4 reduced to approximately zero from 2000 to 2006 [57], a consequence of the production and loss processes being in quasi-equilibrium. Atmospheric growth has since returned to values observed in the second half of the 20th century [39,40] and more recently has increased at a faster rate. There is extensive debate in the literature about which sources are responsible for these recent observed global-scale changes [23,32,33,36,60,66,74], with some studies emphasizing that variations in the OH could also be responsible but this appears to be unlikely given the behaviour of other trace gases that are oxidized by OH [58,68]. A more likely scenario is that some combination of emission and loss variations are responsible for observed atmospheric variations in CH_4.

Calibrated atmospheric CH_4 surface measurements have been collected across the globe (Figure 1a) by a variety of groups, the most extensive network of which is coordinated by the US National Oceanic and Atmospheric Administration (NOAA) since the 1980s. The original purpose of these measurements was to observe large-scale changes driven by natural and anthropogenic emissions, although the network has grown with time and a growing body of work (including this study) have used these data to infer continental-scale emission estimates. The preponderance of these measurement sites, taking advantage of sites established to collect CO_2 measurements, are over North America and Europe and that has implications for understanding sub-continental changes in CH_4 emissions. Colocated measurements of CH_4 isotopologues provide additional information with which to improve source attribution (e.g., [39,56,60–62,76]). In particular, progressively lighter measurements of $\delta^{13}C_{CH4}$ suggest that recent changes in atmospheric CH_4 are due to increased biological activity, e.g. [9,39,60].

Data from the European SCIAMACHY (SCanning Imaging Absorption spectroMeter for Atmospheric CartograpHY) satellite instrument [8], launched in 2002, were the first space-borne measurements that were sensitive to changes in boundary layer CH_4 [10]. Serious degradation of

detector pixels from the end of 2005 compromised these data for quantifying regional CH_4 fluxes [16], although they provided invaluable information about year-to-year variations in atmospheric CH_4 [4]. The Japanese Greenhouse gases Observing SATellite (GOSAT) has collected data since it was launched in 2009 [27]. The main advantage of using satellite data is the global coverage they provide (Figure 1b,d), although instruments are typically in a sun-synchronous orbit so they sample the atmosphere at one local time of the sunlit day. The SWIR wavelengths used to determine CH_4 columns that are sensitive to the lower troposphere are also sensitive to clouds so columns are usually only retrieved in cloud-free scenes, and the columns are difficult to interpret without a model of atmospheric chemistry and transport. Ground-based upward looking spectrometers, e.g., the Total Carbon Column Observing Network (TCCON, Figure 1), play an ongoing key role in ensuring the accuracy of the satellite data [75]. Nevertheless, GOSAT data have significantly revised our understanding of regional CH_4 budgets across the globe, e.g. [15,17,20,25,32,33,37,47,50,67,72,78]. These include studies focused over the tropics where we have little other data available to revise our *a priori* knowledge, e.g. [15,20,32,33,37,72,78], for which in some examples the inferred emissions can be linked to specific source types, e.g., [32,33,37,53,72].

There remain many outstanding science questions associated with CH_4 emissions, some of which are emerging as we witness more frequent anomalous climate variations while others are associated with our ability to detect changes in atmospheric CH_4 that correspond to national net zero pledges. The ability of satellite data to help address these science questions will progressively improve with the length and density of data records, as newer instruments with improved detector technology and better spatial resolution become available. Here we take advantage of the decadal record of CH_4 column data from GOSAT to explore the value of these data over and above the information provided by the NOAA *in situ* network, described in section 2, to understand CH_4 emissions on global to subcontinental spatial scales. We achieve this by inferring CH_4 emissions from these data using common *a priori* inventories, and a common atmospheric chemistry transport model and ensemble Kalman filter inverse method, which are all described in section 2. In section 3 we report *a priori* and *a posteriori* CH_4 fluxes inferred from NOAA and GOSAT CH_4 data on global and continental spatial scales, with a specific focus on tropical South America and the Indian subcontinent. We conclude this section by examining the potential of finer resolution CH_4 data from the European TROPospheric Monitoring Instrument (TROPOMI) by quantifying diffuse coal mining emissions of CH_4 over Northern Queensland, Australia. We conclude the paper in section 4.

2. Data and Methods

(a) In situ Mole Fraction CH_4 Data

We use biweekly CH_4 values determined from measurements of discrete air samples collected in flasks and from continuous online analysers from across the NOAA Cooperative Global Air Sampling Network (Figure 1)

We also use CO_2 measurements as part of our novel analysis of GOSAT CH_4 proxy data, as described below. We use (weekly) discrete flask air samples from 105 sites and (hourly) continuous observations from 52 sites that are part of the global atmospheric surface CO_2 observations network. These are currently described by the Observation Package (ObsPack) obspack_co2_1_GLOBALVIEWplus_v4.1_2018-10-29 data product provided by the NOAA Global Monitoring Laboratory.

(b) Satellite Data

We use data from the GOSAT instrument for our comparative analysis with NOAA *in situ* data, and data from TROPOMI to show how finer spatially resolved data can be used to infer diffuse emissions of CH_4 from coal mining. Methane columns for GOSAT and TROPOMI (Table 1) take

advantage of SWIR wavelengths that are sensitive to changes in CH_4 in the lower troposphere but also sensitive to cloud coverage so that we use only cloud-free scenes.

Greenhouse gases Observing SATellite CH_4 Column Measurements

GOSAT was launched in 2009 by the Japanese Space Agency (JAXA), in collaboration with the Japanese National Institute for Environmental Studies and the Ministry of Environment. The satellite is equipped with a high-resolution Fourier transform spectrometer (TANSO-FTS) that enables the measurement of concentrations of both CO_2 and CH_4. GOSAT is in a sun-synchronous orbit, with a local equator crossing time of 13:00. The instrument has a ground footprint with diameter of 10.5 km with a pixel spacing of approximately 250 km. GOSAT achieve approximate global coverage in three days.

We use GOSAT proxy column methane (XCH4) data from the University of Leicester (version 9.0) [49,51], which has been validated against data from the TCCON network [50] and occasionally using regional aircraft data (e.g. [71]. The proxy XCH4 retrieval simultaneously retrieves CH_4 and CO_2 columns using absorption features around the wavelength of 1.6 μm. These columns are most sensitive to changes in CO_2 and CH_4 in the lower troposphere, where variations are sensitive to surface fluxes. Taking the ratio of these retrieved columns, CH_4/CO_2, effectively assumes CO_2 is a proxy for modifications along the light path [16] and minimizes the influence of common factors that affect the retrieval of both gases, e.g., clouds and atmospheric scattering. Consequently, these ratios are less sensitive against scattering than a full-physics retrieval approach [11], resulting in higher data density over geographical regions where there is substantial aerosol loading, e.g., tropical dry seasons. Analyses have shown that these retrievals have a bias of 0.2%, with a single sounding precision of about 0.72% [50–52].

The conventional approach is then to scale the ratio with an independent estimate for the CO_2 column, often from a model, to infer CH_4 columns. This ratio is used to determine CH_4 rather than CO_2 because it is generally assumed that CO_2 varies much less than CH_4. But of course our knowledge of CO_2 is incomplete (e.g., [12,30,46]), particularly over the tropics, so this last step introduces an unnecessary systematic error to the resulting CH_4 columns [50]. We use an alternative approach, which we previously developed, to directly use the CH_4/CO_2 by taking advantage of sparsely distributed *in situ* that help anchor the GOSAT ratio data, allowing us to simultaneously infer CH_4 and CO_2 fluxes [15,17].

TROPOspheric Monitoring Instrument CH_4 Column Measurements

The TROPospheric Monitoring Instrument (TROPOMI) on board the Sentinel-5p satellite was launched in 2017. The satellite is in a sun-synchronous orbit with a local equator crossing time of 13:30. With a swath width of around 2600 km it provides complete daily coverage of the globe at 5.5×7 km^2 resolution, upgraded from 7×7 km^2 in August 2019. The spectral range of TROPOMI precludes using the proxy retrieval approach so CH_4 columns are determined by a full-physics approach that uses the CH_4 absorption features around the wavelength of 2.3 μm [11,24,31], which takes into account aerosol and cloud scattering. We use the scientific CH_4 data product [31]. These data include an *a posteriori* correction based on TROPOMI data to account for biases at high and low albedos, following [43]. These column data have been validated against TCCON and GOSAT data, with a mean bias (standard deviation) with TCCON of -3.4 (5.6) ppb, and values of -10.3 (16.8 ppb) compared to GOSAT [31].

(c) GEOS-Chem Global 3-D Atmospheric Chemistry Transport Model

For the experiments reported here, we use the GEOS-Chem atmospheric chemistry and transport model at a horizontal resolution of 4° (latitude) × 5° (longitude), driven by the MERRA-2 meteorological re-analyses from the Global Modeling and Assimilation Office Global Circulation Model based at NASA Goddard Space Flight Center. This model is used to relate *a priori* emissions

to 4-D atmospheric fields of CH_4. We also describe *a priori* fluxes for CO_2 that we need to infer simultaneously fluxes of CH_4 and CO_2.

Our *a priori* CO_2 flux inventory includes: 1) monthly biomass burning emission (GFEDv4.1; [69]; 2) monthly fossil fuel emissions (ODIAC; [42]; 3) monthly climatological ocean fluxes [65]; and 4) 3-hourly terrestrial biosphere fluxes (CASA; [44]. Our CO_2 model calculations follow closely a recent study [46]. Our *a priori* CH_4 fluxes from nature include: 1) monthly WetCHARTS v1.0 wetland emissions, including rice paddies [6]; 2) monthly fire CH_4 emissions are from GFEDv4.0; 3) termite emissions [19]. Emissions from geological macroseeps are based on [14] and [28]. For areal seepage, we use the sedimentary basins (microseepage) and potential geothermal seepage maps [28] with the emission factor described by [34]. For *a priori* anthropogenic emissions we use the EDGAR v4.41 global emission inventory [26] that includes various sources related to human activities (e.g., oil and gas industry, coal mining, livestock, and waste). We use monthly 3-D fields of the hydroxyl radical, consistent with observed values for the lifetime of methyl chloroform, from the GEOS-Chem HOx-NOx-Ox chemistry simulation [35,67] to describe the main loss of tropospheric CH_4 [18] and the loss of CH_4 in the stratosphere. Using fixed, archived field of OH allows us to linearly decompose total CH_4 into contributions from individual sources and geographical regions. We also include a simple soil sink of CH_4 [18].

(d) Ensemble Kalman Filter Inverse Method

We use an ensemble Kalman Filter (EnKF) framework [15] to estimate simultaneously CO_2 and CH_4 fluxes from and satellite measurements of the atmospheric CO_2 and CH_4 from 2009 to 2019, inclusively. For these experiments we report net CH_4 emission estimates and do not attempt to distinguish emissions from individual sectors.

Our state vector includes monthly scaling factors for 486 regional pulse-like basis functions that describe CO_2 and CH_4 fluxes, including 476 land regions and 11 oceanic regions. We define our land sub-regions by dividing the 11 TransCom-3 [22] land regions into 42 nearly equal sub-regions, with the exception for temperate Eurasia that has been divided into 56 sub-regions due to its large landmass. We use the 11 oceanic regions defined by the TransCom-3 experiment.

We assume the *a posteriori* CH_4 or CO_2 flux estimate takes the form [15]:

$$f_p^g(x,t) = f_0^g(x,t) + \sum_i c_i^g BF_i^g(x,t), \tag{2.1}$$

where g denotes the atmospheric concentration of CH_4 or CO_2 and $f_0^g(x,t)$ and $f_p^g(x,t)$ describe their *a priori* and *a posteriori* flux inventories, respectively. The pulse-like basis functions $BF_i^g(x,t)$ represent the sum of different source sectors, which we use to represent their overall spatial pattern for each month over each sub-region. c_i^g denotes the state vector that comprises of scaling factors. As a result, we estimate a total of 104,976 (i.e., 2 (CH_4 or CO_2) $\times$ 108 (months) $\times$ 486 (sub-regions)) coefficients, by optimally fitting model concentrations with observations [15]. For further details we refer the reader to [15].

We assume a fixed uncertainty of 40% for coefficients corresponding to *a priori* CO_2 fluxes over each sub-region, and a larger uncertainty (60%) for the corresponding CH_4 emissions. We also assume that *a priori* errors for the same gas are correlated with a spatial correlation length of 600 km and with a temporal correlation of one month. We also assume that each single GOSAT proxy XCH4:XCO2 ratio retrieval has an uncertainty of 1.2% to account for possible model errors, including the errors in atmospheric chemistry and transport. We assume uncertainties of 0.5 ppm and 8 ppb for the NOAA *in situ* observations of CO_2 and CH_4, respectively. Following our previous work [15], we assume a model error of 1.5 ppm and 12 ppb for CO_2 and CH_4, respectively. We adopt a larger percentage value for the CH_4 model error to account for difficulties in modelling chemical sinks of atmospheric CH_4 [18,54].

3. Results

Here we report global CH_4 fluxes and how they vary across zonal bands, progressively ascribing values to smaller geographical regions. For the sake of brevity, we focus our attention on a few geographical regions and refer the reader to other papers dedicated to changes elsewhere (e.g., [20,32,33,37,73]). We also highlight the ability of the newer TROPOMI instrument to identify example diffuse emissions from Australian coal mining.

(a) Global and Continental Net CH_4 Budgets

Figure 2a and Table 2 show global emission budgets inferred using NOAA *in situ* and GOSAT CH_4 from a common *a priori* estimate. Generally, we find that the global annual *a posteriori* estimates are within 1% of *a priori* values at the start of the decade and typically higher by 5% ($\simeq$30 Tg) after 2014. This difference increases to 10–20% after 2014 for tropical *a posteriori* estimates. Figure 2a shows that this annual increase mainly reflects changes during boreal summer months. There are also differences between *a priori* and *a posteriori* values during austral summer months but they are generally smaller. On this global scale, there is excellent agreement ($<$1%) between emissions inferred from *in situ* and GOSAT data, as expected, as they are determined by global mass balance.

Figure 2b shows the *a priori* and *a posteriori* statistics of annual CH_4 fluxes integrated over 30° zonal bins. We find agreement in the broad latitudinal distribution of CH_4 fluxes. The largest fluxes are found in the northern tropics, northern extratropics (30°N–60°N), and the southern tropics. Emissions from the poles and southern extratropics are comparatively small. Again, the two sets of *a posteriori* estimates are statistically consistent, with increases relative to the *a priori* in the tropics and a decrease in the northern extratropics. Figure 2c shows annual anomalies relative to the corresponding the *a priori* and *a posteriori* 2010–2019 annual mean values. The largest anomalies are over the southern tropics (0°S–30°S) and the northern tropics, with significant variations over the northern extratropics and northern pole. The NOAA *a posteriori* fluxes show the largest relative variations over the northern tropics and GOSAT shows the largest relative variations over the southern tropics.

Figure 3 shows the Siegel linear trends for *a priori* and *a posteriori* CH_4 fluxes during 2010–2019 and during the second half of that decade to minimize the impact of the El Niño. We use the Seigel non-parametric estimator [63] to fit a line to our data because the method is less sensitive to outliers that would otherwise compromise the linear trend estimate and the resulting estimated trend has a lower variances; we find similar trend estimates using the Theil-Sen estimator. In our 2010–2019 calculations (n = 120), we want to estimate the secular trend without considering the large-scale perturbation from, for example, the 2014–2016 El Niño. By definition this approach also removes large CH_4 pulses that we have previously attributed to anomalous precipitation [33]. We discard trends with an absolute value $<$0.025 Tg CH_4/yr yr^{-1} to focus on the largest positive and negative trends. We find that there are small, localized *a priori* trends that are mainly associated with fire inventories that are already influenced by satellite data. In contrast, our *a posteriori* fluxes 2010–2019 (Figures 3c,e) show large positive and negative trends across the tropics, particular over tropical South America, Central Africa, India, and southern China. Trends are generally larger for GOSAT, but their broad distribution is similar for both NOAA and GOSAT, which is remarkable given the comparatively small number of NOAA data over the tropics.

When we consider only the second half of the decade (2016–2019, n = 48) we find that the trends over the tropics are larger and there are more extra-tropical regions with trends $>$0.025 Tg CH_4/yr yr^{-1} (Figures 3d,f). In contrast, trends driven by the *a priori* inventories (Figures 3b) are mostly limited to small geographic regions over North America and Siberia. We also find broad geographical agreement between *a posteriori* fluxes inferred from NOAA and GOSAT data, although there are differences in the magnitude of trends (e.g. India) and there is widespread discrepancy across tropical South America and Australia. The largest negative trend

is over Russia, west of the Ob River. We now investigate in more detail the temporal variations in estimated fluxes over India and tropical South America.

(b) Tropical South America

Figure 4a shows the monthly and annual timeseries of *a priori* and *a posteriori* CH_4 fluxes (Tg/yr) over tropical South America (broadly defined by 30–85°W, -20°S–13°N) from 2010 to 2019; the corresponding annual values are also reported in Table 2. Even on this large spatial scale there are periods of substantial deviation from fluxes inferred from NOAA and GOSAT and the commmon *a priori* inventory, most notably during the 2014–2016 El Niño, suggesting both these data contain information about this broad geographical region. We find a strong seasonal cycle of CH_4 emissions, particularly at equatorial latitudes (Figure 4b), that peaks in the first half of each calendar year and is driven by rain-fed wetland emissions. This seasonal cycle is less obvious for the regional monthly means (Figure 4a).

Broadly, below the equator, GOSAT *a posteriori* fluxes are higher than fluxes inferred from NOAA data in the first half of each calendar year, usually dominated by wetland emissions during regional wet seasons, and lower during the second half of the calendar year when emissions are dominated by dry-season fire emissions that tend to be further south. Above the equator, we find the highest emissions are during the second half of the year and focused over the Orinoco River floodplain that spans Venezuela and Colombia.

The 2010 CH_4 pulse represents the largest anomaly in the decadal record for emissions over Tropical South America inferred from NOAA (Figures 4b,c) and for GOSAT (Figure 4e), but the distribution of these pulses are spatially distinct from each other (Figure 4d) and from the *a priori* inventory (not shown). The spatial distribution of the CH_4 pulse during August–September 2010 inferred from GOSAT data is focused over the Amazon forest that intersects the Brazilian states of Goiás, Tocantins, and Mato Grosso, and the Bolivian portion of the Amazon forest, closely resembles the distribution of maximum climatological water deficit that has been used previously as a metric for drought intensity [29] and likely due to elevated fire emissions.

The spatial distribution of elevated *a posteriori* emissions inferred from NOAA and GOSAT data during February–April 2019 closely follow the *a priori* inventory for wetlands, focused over Ilha de Marajó in the Brazilian state of Pará; Iquitos, Peru; following the Amazon river across the Brazilian state of Amazonas; and along the northern section of the Beni River in Bolivia. We do not currently have an explanation for this pattern of elevated emissions during early 2019. We find no evidence for elevated rainfall, surface temperatures, or fires. Variations in wetland emissions of CH_4 are also driven by changes in the carbon supply that supports methanogenesis. So that a plausible explanation for higher CH_4 emissions in 2019 is that elevated fire activity from the previous dry season increased the pool of carbon available for methanogenesis (per. comm.: A. A. Bloom, JPL, May 2021), but further data are needed to improve understanding of the biogeochemical processes that control Amazonian wetland emissions of CH_4 [7].

(c) Indian Subcontinent

Figure 5a shows the monthly and annual timeseries of *a priori* and *a posteriori* CH_4 fluxes (Tg/yr) over the Indian subcontinent (broadly defined by 65–95°E, 5–35°N), which includes parts of Pakistan, Bangladesh, Bhutan, and western Myanmar. Annual values are also reported in Table 2. There is a clear regional seasonal cycle that peaks during July–October over the region broadly defined by 20–30°N (Figure 5b) and 75–85°E (centred over Utter Pradesh) consistent with the main Kharif rice growing season that is sown in June–July and harvested in November–December. The timing of the peak is consistent with these rice plants being sufficiently mature during July–October to allow effective transmission of CH_4, produced by rhizospheric methanogens, through their aerenchyma [1]; we acknowledge that current knowledge about plant-mediated transport of CH_4 remains incomplete due to lack of convenient collection methods [5].

Generally, *a posteriori* estimates deviate from *a priori* estimates throughout the year with the largest values during January–October (Figure 5a). *A posteriori* CH_4 emission estimates inferred from GOSAT tend to be larger than *a priori* estimates during the peak of the seasonal cycle over Utter Pradesh, as described above, and comparable or slightly smaller at the seasonal trough. We find that *a posteriori* flux estimates inferred from NOAA show less year to year variability in the seasonal peaks than those inferred from GOSAT data (Figure 5a,d), although their monthly anomalies with respect to their own 2010–2019 mean show some consistency during periods when the regional seasonal peaks are at their largest (Figure 5c,e), e.g. during the El Niño period and 2017. In general, our year to year variations in CH_4 fluxes up until 2015 are more consistent with those from [37] than [20]. Since 2017, GOSAT fluxes (and to a lesser extent NOAA fluxes) show a step-wise increase in emissions (Figure 3) over Northest India and northern Bangladesh, although the resolution of our *a posteriori* fluxes precludes further localization. Seasonal flooding, changes in rice production, and increased coal mining to support growing national energy demands are potential culprits but further investigation of this observation is outside the scope of this study.

(d) New Satellite Data Allows Hotspot Mapping: Australian Case Study

Satellite observations from the TROPOMI satellite provide daily global spatial coverage, subject to cloud cover and aerosol loading, at higher spatial resolution than previous Earth-orbiting sensors (Figure 1). This high spatial resolution allows us to focus on smaller source regions or even large individual emitters of CH_4. There are many examples in the literature that use TROPOMI data in this way, particularly focused on the oil and gas sector that is an exemplar of a large point source of CH_4 [13,48,70,77]. These studies have largely focused on the use of individual overpasses and plumes of CH_4 measured by TROPOMI on certain days. However, cloud coverage can hinder regular observations of a particular source and even at the 5.5×7 km resolution of TROPOMI, the underlying source may not be resolved because the emission rate corresponds to a CH_4 column perturbation comparable to the measurement noise in which case combining measurements collected successively over a region is required.

We demonstrate the capability of TROPOMI data to observe ands quantify emissions on the scale of large individual coal mines. We focus on the Bowen basin region of Queensland (QLD), Australia (Figure 6). Data from individual overpasses indicate the presence of significant CH_4 sources within the Bowen basin. However, as a region containing over 40 coal mines, it is not clear from where exactly the high CH_4 concentrations emanate. To resolve this, we use a temporal oversampling approach [64,79] to average CH_4 column data collected from individual overpasses onto a regular fine resolution grid (in our example, $0.02^\circ \times 0.02^\circ$) to isolate the major sources of emissions within the Bowen basin. We use a simple point radius based approach to the temporal oversampling, following [79]. For each 0.02° target grid cell we find all TROPOMI pixels whose centre is within 5 km of the centre of the target grid cell. We then use one year of data to build up a $0.02^\circ \times 0.02^\circ$ grid of CH_4 concentrations during 2019.

Figure 6 shows the oversampled TROPOMI data over the northern part of the Bowen basin. Clear CH_4 enhancements of up to 20 ppb are seen over several sets of coal mines. These mines are identified in the figure as Moranbah North / Broadmeadow (MN), Hail Creek (HC), Coppabella (CB) and Capcoal (CC). The oversampled data demonstrate the ability of TROPOMI to isolate large sources of emissions such as these mines.

To quantify the annual mean CH_4 emissions from each of these mines we use a simple mass balance approach, following [25]. Given an enhancement in atmospheric CH_4 column (ΔX) over a source region, the emissions rate, Q, can be defined as:

$$Q = \frac{\Delta X M_{CH4} U W p}{M_{atm} g}, \tag{3.1}$$

where U is the mean 10 m wind speed, W is the size of the box, p is the dry atmospheric surface pressure, g is the gravitational constant and the M_x terms represent the molar mass of CH_4 and the atmosphere. We use values of U and p from MERRA-2 reanalyses, as used by the GEOS-Chem

model. For this illustrative calculation we do not take into account changes in wind direction over the oversampling period.

Table 3 shows the annual mean emission estimates from each of the selected mines alongside the respective production statistics and reported annual total greenhouse gas emissions, described as CO_2 equivalent values assuming a global warming potential of 28 [38], under the Australian reporting system for national highest emitters. We acknowledge these estimates are not directly equivalent to our CH_4 emissions, but the majority of CO_2-equivalent emissions from coal mines are from CH_4 rather than CO_2 so they can be reasonably compared.

Moranbah North and Capcoal have the largest reported emissions, reflecting that they are underground coal mines that generally emit more CH_4 than surface mines because of the higher gas content of deeper coal seams. Our emission estimates for both these mines are broadly equivalent to the reported total. In contrast, our emission estimates for the two surface mines, Coppabella and Hail Creek, are four and two times larger than the reported amounts, respectively. This discrepancy may reflect large errors in emission factors for surface coal mines. We find that other surface mines in the region do not have similarly detectable CH_4 enhancements, despite having larger total coal production. So our larger emission estimates may also be a result of mine-specific activities or enhanced gas content in these particular coal seams. We also acknowledge that our estimates have large uncertainties that reflect uncertainties associated with the assumed uniform wind speed, quantifying the CH_4 column enhancement relative to the local background, and the definition of each source region. Some of these uncertainties could be reduced by using a high-resolution 3-D meteorological model but nevertheless the enhancements over the Bowen basin (Figure 6) demonstrate the capability of the current generation of satellite data to identify the largest CH_4 emitters so they can be compared with national reporting mechanisms (e.g. [21]).

4. Concluding Remarks

We have shown that the added value of satellite data for understanding the contemporary CH_4 budget is mainly from its superior spatial coverage, particularly over the tropics where there are very few *in situ* measurements. On a global scale we find excellent agreement between CH_4 fluxes estimated using data collected by the NOAA surface network and by the Japanese Greenhouse gases Observing SATellite (GOSAT), as expected. Differences begin to appear when these *a posteriori* fluxes are described on 30° latitudinal bins but they are mostly within the associated *a posteriori* uncertainties. Even on large continental scales, long-term trends (2010–2019) in emissions from NOAA and GOSAT data are mostly consistent. It is only when we investigate shorter term variations and sub-continental spatial scales that we see a significant discrepancy between the distribution and magnitude of CH_4 flux estimates. We demonstrate this by examining fluxes over tropical South America and the Indian subcontinent, regions that have recently experienced large-scale climate perturbations. Recent increases in the global atmospheric CH_4 growth rate are linked to large and rapid changes in emission sources, particularly over tropical continents where GOSAT can provide more spatially resolved information than NOAA data.

For the sake of brevity, we have limited our analysis to CH_4 column data and consulted other data as part of the narrative. In practice, we have a wealth of *in situ* and satellite data to help attribute observed changes in CH_4 to changes in fire, hydrology, anthropogenic emissions [45]. Integrating those auxiliary data into a coherent narrative about changing CH_4 emissions is already possible. Formal integrating data that describe the carbon cycle and water, for example, within a Bayesian framework represents an important next step for the community. Only with this approach can we move towards a more process-level understanding of, say, wetland emissions that can then be challenged and developed with targeted fieldwork measurements. This formal approach requires that we characterize the error budget of the remotely sensed data, which requires a sustainable and transparent ground-truthing framework (e.g. [2,3,75]).

Newer instruments such as TROPOMI that have better daily coverage and finer spatial resolution open up new research directions. For example, we used these data to estimate

diffuse emissions from Australian coal mines. Other groups have already started using these data to study emissions from large urban centres, power plants that effectively represent large, fixed-point sources, and to improve understanding the controls of wetland emissions, moving beyond what can be achieved using GOSAT. The next generation of satellite instruments, e.g., GHGSat (https://www.ghgsat.com/), MethaneSat (https://www.methanesat.org/), Space Carbon Observatory (https://scarbo-h2020.eu/), and the constellation of sensors aboard the Copernicus CO_2 service, will dramatically increase the volume of high spatial resolution quality CH_4 data.

The grand challenge is to use data to improve predictive Earth system models so we can use them to better understand what is in store for us and to develop effective climate policy (Figure 7). To achieve the necessary but ambitious goals of the Paris Agreement requires that we understand emissions from human ecosystems (e.g., urban centres, oil and gas industry, food production) *and* natural ecosystems (e.g., wetlands). They represent complementary measurement and analysis challenges. On spatial scales of our largest cities (<100 km) we need to make better use of new technology alongside more established instruments. We suggest that the internet of things should incorporate environmental measurements, taking advantage of fixed (e.g. buildings) and moving (e.g. transport) urban structures. Individual small-scale atmospheric sensors are less accurate and precise than research-grade equipment, but AI network algorithms can help integrate sensor kilo- or mega-clusters (calibrated with gold-standard equipment) to describe CH_4 (and CO_2) variations associated with the continual movement of millions of people. Machine-learning techniques will be important to infer surface carbon fluxes from the unprecedented volumes of data. A sustainable global observing system requires a business model. We propose that the global scale observing backbone, delivered by calibrated ground-based networks and satellites, should be funded by public money, reflecting the climate commons. Urban ecosystem measurement systems, including commercial satellites, should be funded by emitters and climate finance and by potential customers, e.g., insurance industry and hedge funds, to promote decarbonization projects. More accurate information about city emission trends will help create new markets that are not covered by current carbon trading schemes.

It is encouraging that most of the technological and scientific expertise necessary to address our challenges already exists in different disciplines and sectors (Figure 7). Part of our transformational challenge will be how to harness that expertise. Meeting the demands of the Paris Agreement also requires major structural changes in the way we live, the way we produce and consume energy, and the way we do business. Collectively, these will be generation-defining changes.

Ethics. No methane molecules were harmed in our experiments.

Data Accessibility. All the data and materials used in this study are freely available. The NOAA ObsPack data products (https://esrl.noaa.gov/gmd/ccgg/obspack/) are available subject to their fair use policies. The University of Leicester GOSAT Proxy v9.0 XCH4 data are available from the Centre for Environmental Data Analysis data repository [49]. The presented material contains modified Copernicus TROPOMI CH_4 data, available from ftp://ftp.sron.nl/open-access-data-2/TROPOMI/tropomi/ch4/. The GEOS-Chem model code is available at http://acmg.seas.harvard.edu/geos/.

Authors' Contributions. P.I.P., L.F., and M.F.L. contributed equally to the data analysis presented in this paper, P.I.P. led the writing of the paper with contributions from coauthors L.F., M.F.L., R.J.P., H.B., X.L., A.L., and T.B..

Competing Interests. The authors declare that they have no competing interests.

Funding. P.I.P., L.F., R.J.P. and H.B. acknowledge support from the UK National Centre for Earth Observation funded by the National Environment Research Council (NE/R016518/1); P.I.P. and M.F.L. acknowledges funding from the Methane Observations and Yearly Assessments (MOYA) project (NE/N015916/1); R.J.P. and H.B. also acknowledge funding from grant NE/N018079/1.

Acknowledgements. We thank all the scientists that submitted data to the CO_2 and CH_4 Observation Package (ObsPack) data products, coordinated by NOAA GML, and making them freely available for carbon

cycle research. We thank the Japanese Aerospace Exploration Agency, National Institute for Environmental Studies and the Ministry of Environment for the GOSAT data and their continuous support as part of the Joint Research Agreements at the Universities of Edinburgh and Leicester. This research used the ALICE High Performance Computing Facility at the University of Leicester for the GOSAT retrievals. The TROPOMI data processing was carried out on the Dutch National e-Infrastructure with the support of the SURF Cooperative. We also thank the GEOS-Chem community, particularly the team at Harvard who help maintain the GEOS-Chem model, and the NASA Global Modeling and Assimilation Office (GMAO) who provide the MERRA 2 data product.

Disclaimer. NA.

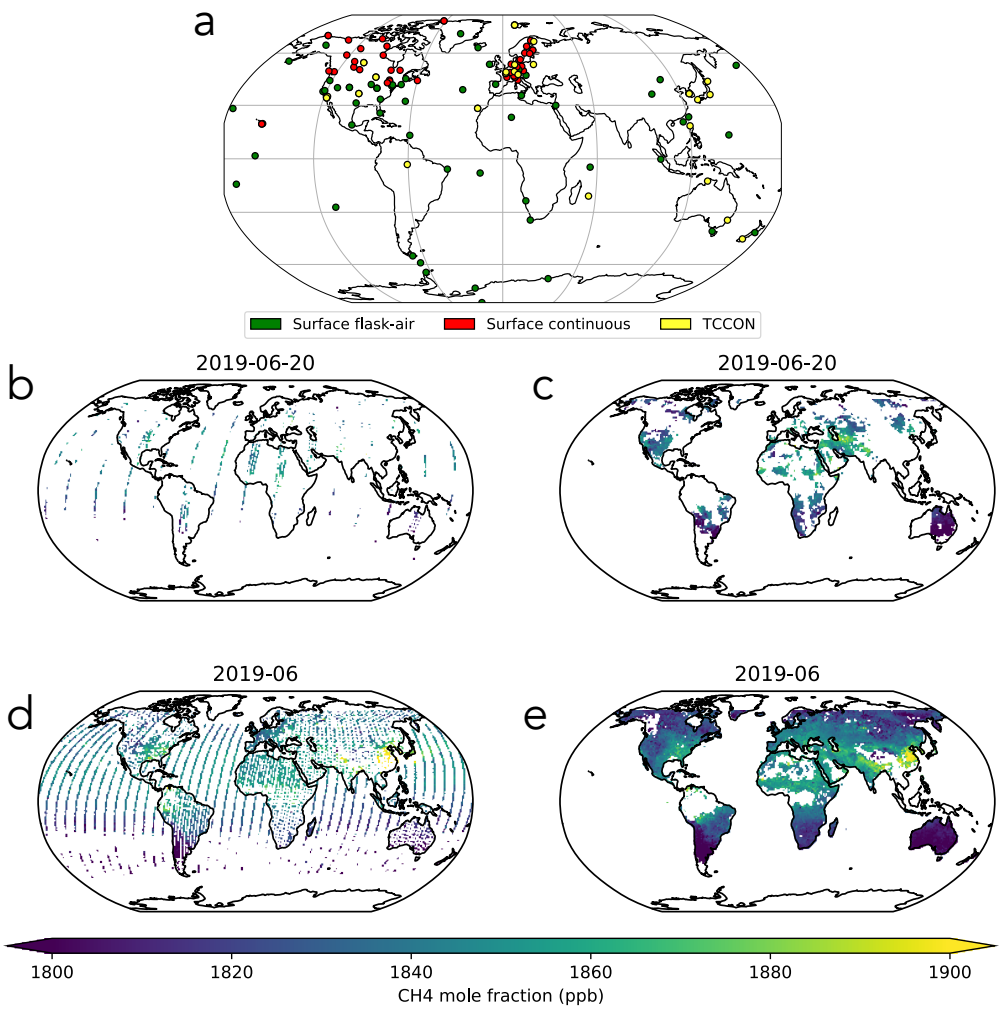

Figure 1. Geographical locations of data collected by a) ground-based measurements operated by NOAA, daily distributions of clear-sky methane columns observed by b) GOSAT and c) TROPOMI satellite instruments on 20th June 2019, and the corresponding monthly distributions for d) GOSAT and e) TROPOMI for June 2019. Ground based measurements include flask measurements (green dots) and *in situ* continuous analyzer measurements (red dots) of CH_4 operated by NOAA, a subset of which we use to determine *a posteriori* flux estimates, and the methane columns measured the Total Carbon Column Observing Network (TCCON, [75]).

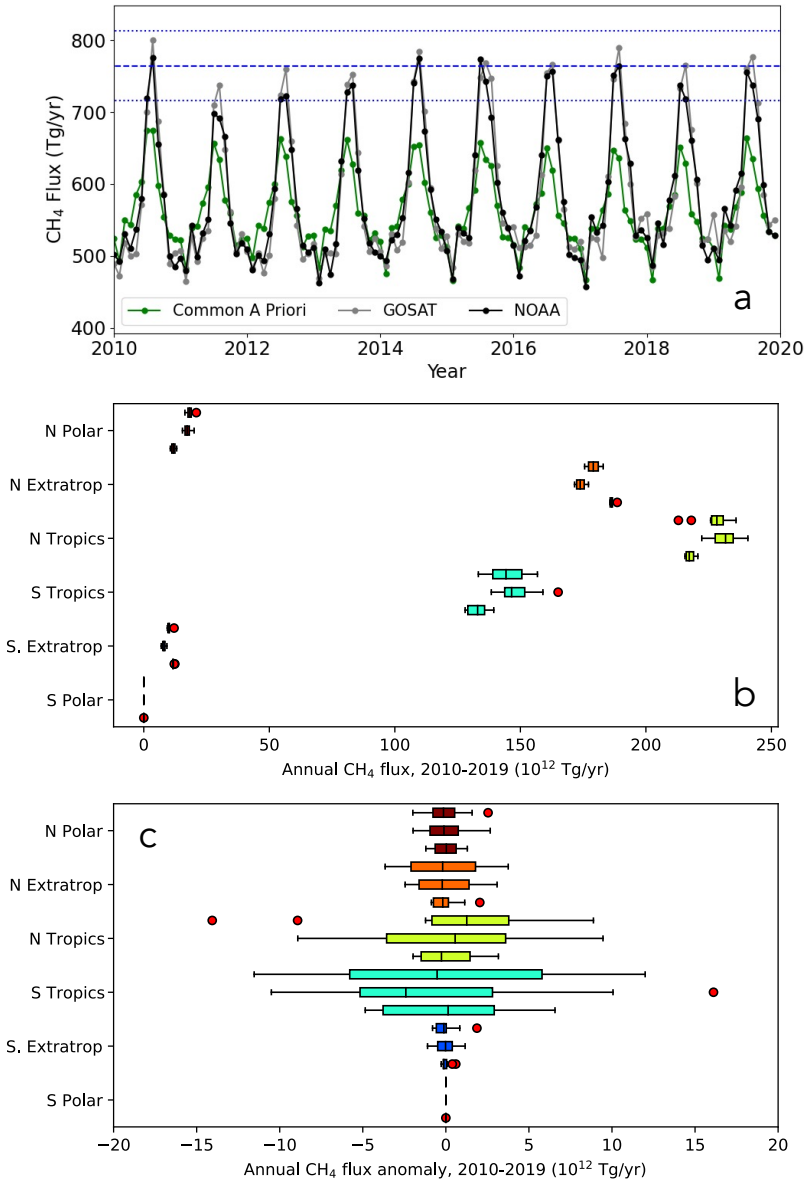

Figure 2. a) Time series of global monthly methane fluxes (Tg/yr) inferred from GOSAT and NOAA methane measurements from 2010 to 2020, and the corresponding common *a priori* values. The corresponding annual methane fluxes (Tg/yr) are reported in Table 2. The blue dashed and dotted horizontal denote the 2010-2019 mean seasonal peak value and the ± 1-σ values, respectively. b) Box and whiskers plot of the annual mean methane fluxes (10^{12} Tg/yr) from 2010 to 2019. The top, middle, and bottom values in each triplet correspond to fluxes inferred from GOSAT and *in situ* data, and to the common *a priori* data. Estimates are described across 30° zonal bands. c) The corresponding annual mean anomalies, calculated by removing the 2010–2019 mean flux from all years. Red dots denote outliers that lie outside $1.5\times$ the inter-quartile range.

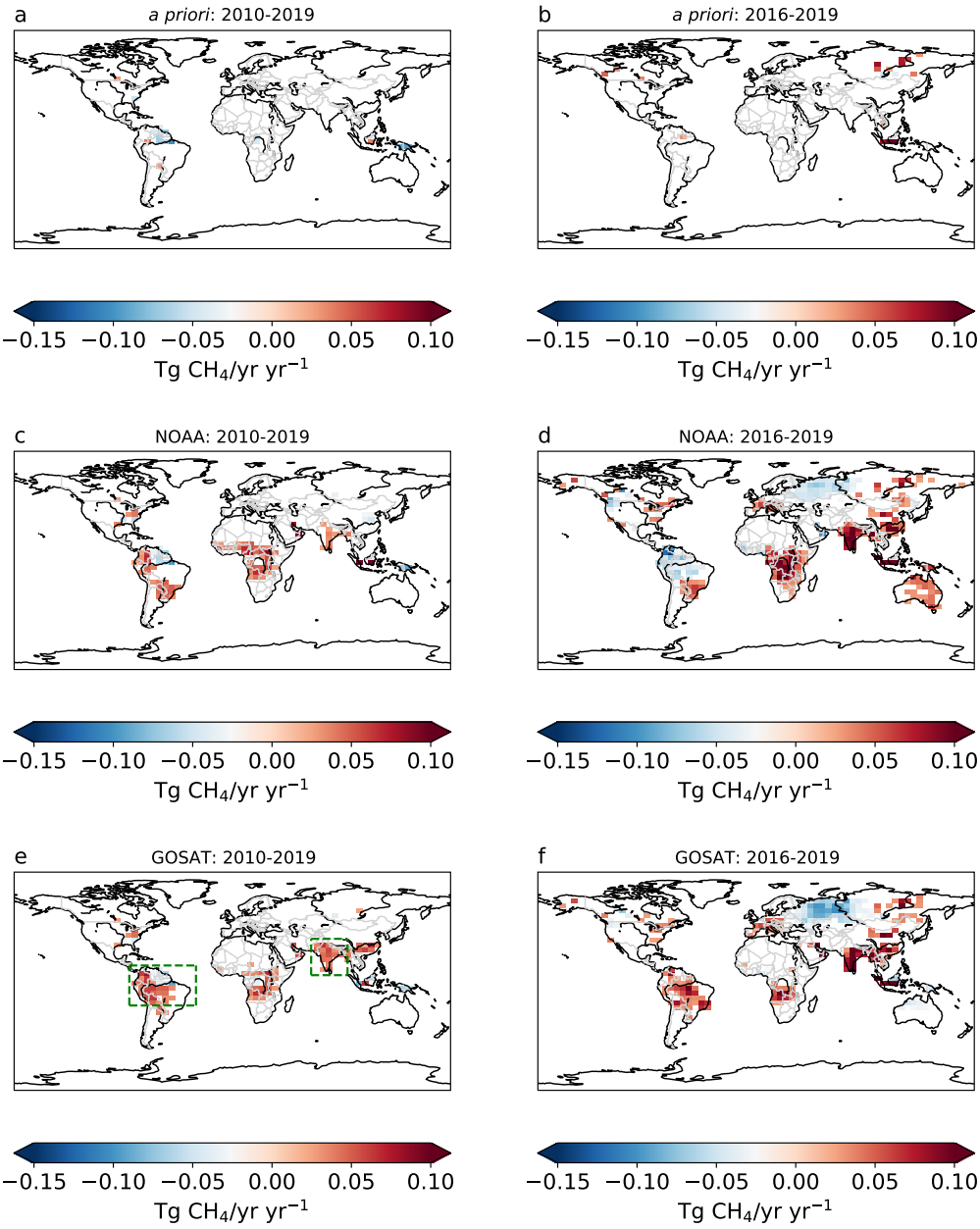

Figure 3. Linear trend estimates, determined by the Siegel repeated median estimator, (Tg CH_4/yr yr^{-1}) of *a posteriori* CH_4 fluxes taken from (top row) *a priori* inventories, and inferred from (middle row) NOAA *in situ* measurements and from (bottom row) GOSAT column data for (left column) 2010–2019 (n = 120) and (right column) 2016–2019 (n = 48). We discard absolute trends $<$ 0.025 Tg CH_4/yr yr^{-1} to emphasize the largest positive and negative trends. Green dashed boxes denote our definitions of tropical South America and the Indian subcontinent used in subsequent analyses.

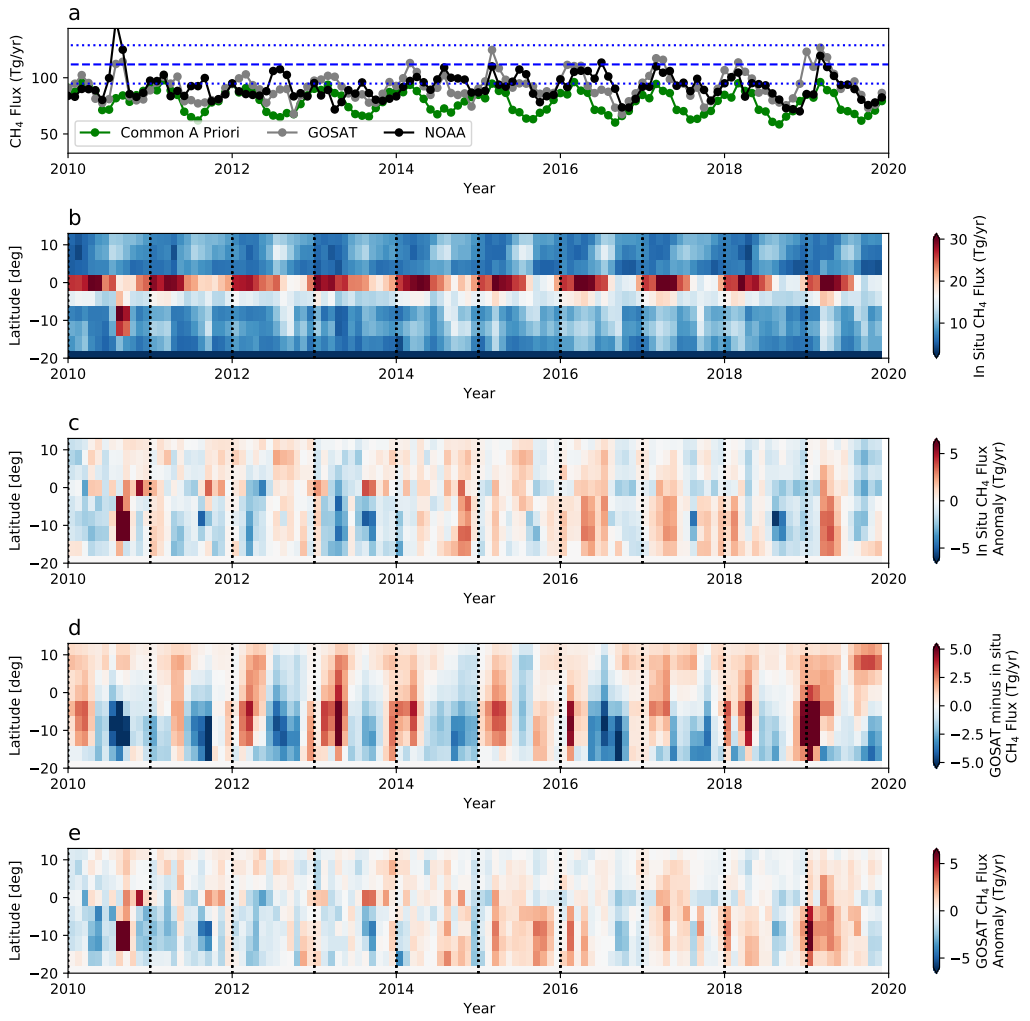

Figure 4. a) Monthly *a priori* and *a posteriori* CH_4 flux estimates (Tg/yr) for tropical South America, (broadly defined by 30–85°W, -20°S–13°N) from 2010 to 2019. *A posteriori* estimates are inferred from (black) NOAA *in situ* measurements (black) and (grey) GOSAT column measurements (grey) using (green) common *a priori* estimates. Corresponding annual flux estimates are denoted by squares. b) *A posteriori* flux estimates inferred from *in situ* data as a latitude-time Hövmoller plot, and c) the corresponding monthly flux anomalies relative to 2010–2019 monthly means. d) Monthly *a posteriori* flux estimates inferred from GOSAT data relative to the monthly *in situ a posteriori* estimates. e) Monthly GOSAT *a posteriori* flux anomalies relative to 2010–2019 monthly means

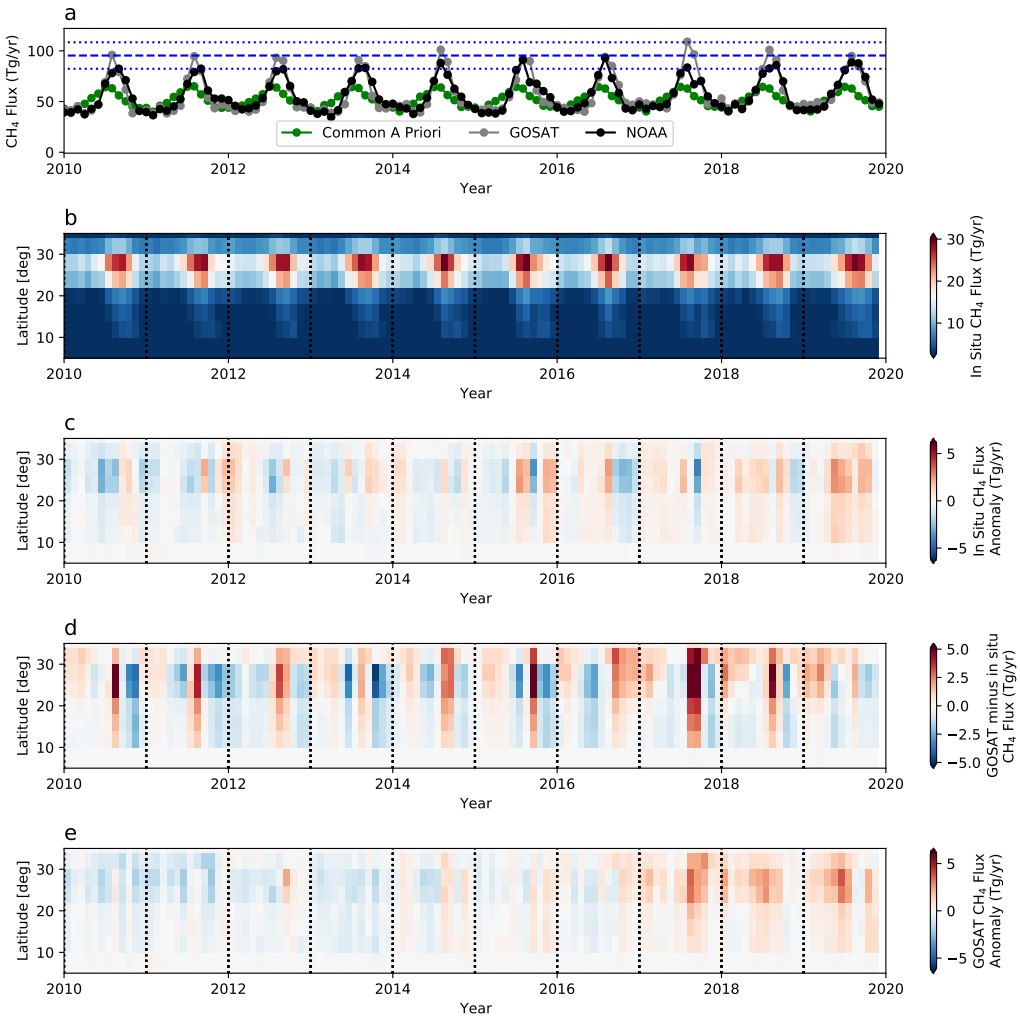

Figure 5. As Figure 4 but for the Indian subcontinent, broadly defined 65–95°E, 5–35°N.

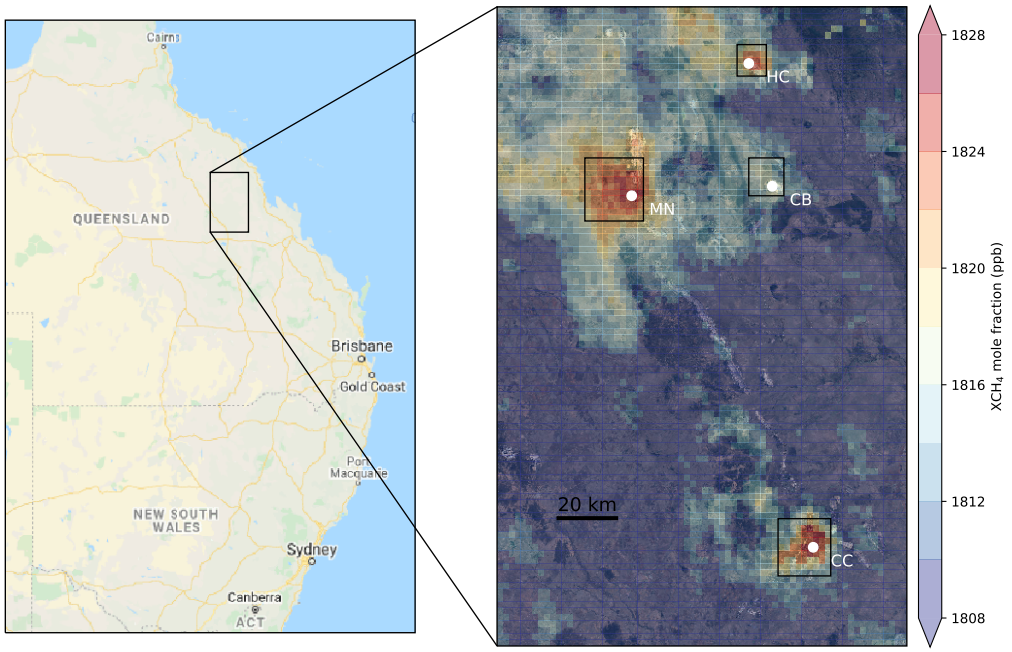

Figure 6. Oversampled TROPOMI column data (ppb) over the Bowen Basin in Queensland, Australia. CB, CC, HC, and MN denote Coppabella, Capcoal, Hail Creek, and Moranbah North/Boradmeadow (MN) mines (Table 3).

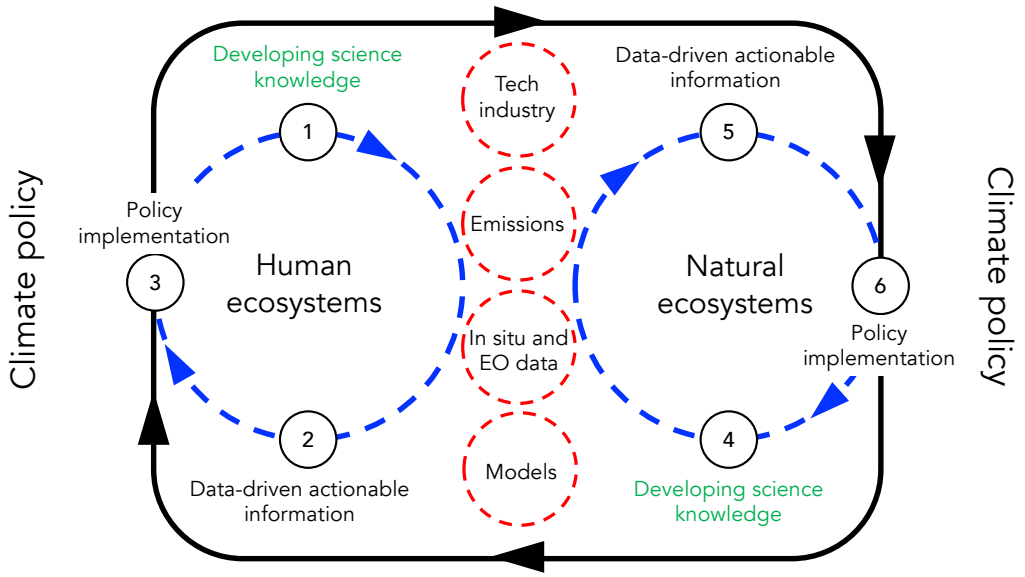

Figure 7. The links and exchanges that need to work to produce data-driven actionable information for the development of climate policy that simultaneously addresses human and natural ecosystem emissions of CH_4.

Instrument	Data Availability	Wavelength coverage	Orbit, LECT, repeat frequency	Ground footprint dimension
SWIR Instruments				
SCIAMACHY (nadir)	2002–2012	SWIR	SS, 1000d, 3	30×60 km^2
GOSAT-1/TANSO	2009–present	SWIR/TIR	SS, 1300d, 3	10.5 km diameter
GOSAT-2/TANSO	2019–present	SWIR/TIR	SS, 1300d, 3	10.5 km diameter
TROPOMI	2018–present	SWIR	SS, 1330a, 1	5.5×7 km^2

Table 1. Satellite instruments that have contributed to our understanding of atmospheric CH_4 and the the corresponding regional distribution of emissions. LECT refers to the local equatorial crossing time and the repeat frequency refers to the approximate time between successive measureements over a particular region, subject to clear-sky criteria.

Year	Annual CH_4 Emissions (Tg/yr)								
	Global			Tropical S. America			Indian Subcontinent		
	A priori	*A posteriori*		*A priori*	*A posteriori*		*A priori*	*A posteriori*	
		In situ	GOSAT		*In situ*	GOSAT		*In situ*	GOSAT
2010	571.0±20.8	572.6±10.4	568.4±6.0	81.3±6.8	91.0±5.3	87.1±3.1	47.8±4.1	50.4±2.4	50.3±1.4
2011	560.1±19.1	560.1±10.2	562.1±5.9	76.9±5.7	86.8±4.8	83.7±3.1	48.5±4.2	51.4±2.5	50.3±1.4
2012	562.6±19.2	565.2±10.0	561.0±5.9	74.6±5.7	87.6±4.8	85.4±3.1	48.4±4.2	53.0±2.5	52.1±1.5
2013	561.0±19.2	563.8±10.0	568.0±5.9	76.3±5.7	82.2±4.8	86.7±3.1	48.6±4.2	51.9±2.5	50.0±1.4
2014	564.8±19.2	590.0±9.9	585.3±5.8	75.9±5.7	91.1±4.8	88.4±3.1	48.3±4.2	52.7±2.4	53.4±1.5
2015	562.9±19.2	593.5±9.7	597.6±5.9	73.4±5.7	88.6±4.9	91.1±3.1	48.7±4.2	53.6±2.4	53.4±1.5
2016	554.5±19.2	583.0±9.9	582.4±5.8	73.6±5.7	90.4±4.8	87.1±3.1	48.9±4.2	52.0±2.4	53.2±1.5
2017	553.7±19.2	588.0±9.9	588.2±5.8	73.1±5.7	89.5±4.8	90.0±3.1	48.8±4.2	54.2±2.5	58.0±1.5
2018	553.5±19.2	582.8±9.9	586.8±6.0	72.4±5.7	83.0±4.8	87.3±3.1	48.8±4.2	54.5±2.5	57.1±1.5
2019	560.5±19.2	597.1±9.9	598.9±6.1	73.4±5.7	85.7±4.8	93.1±3.1	48.8±4.2	57.3±2.5	58.1±1.5

Table 2. Annual *a priori* and *a posteriori* CH_4 fluxes and their 1-σ uncertainties (Tg/yr) for the globe, tropical South America and subcontinental India.

Mine	Type	Annual production (Mt)	Reported emissions (Mt CO_2-eq)	Estimated emissions (Mt CO_2-eq)	ΔXCH_4 (ppb)
Capcoal	Underground & Surface	11.81	2.80	3.1 ± 1.5	17
Moranbah North / Broadmeadow	Underground	13.01	3.18	3.3 ± 1.5	15
Coppabella	Surface	3.61	0.19	0.9 ± 0.4	7
Hail Creek	Surface	7.66	0.50	1.2 ± 0.6	12

Table 3. Production statistics, reported and estimated emissions and TROPOMI annual mean enhancement from selected mines in the Bowen Basin, Queensland, Australia. Coal production statistic are taken from https://www.data.qld.gov.au/dataset/coal-industry-review-statistical-tables, last accessed 26th March 2021. CO_2-equivalents are calculated using a GWP of 28 from IPCC AR5.

References

1. M. S. Aulakh, J. Bodenbender, R. Wassmann, and H. Rennenberg.
   Methane transport capacity of rice plants. i. influence of methane concentration and growth stage analyzed with an automated measuring system.
   Nutrient Cycling in Agroecosystems, 58(1):357–366, 2000.
2. Pinty B., P. Ciais, D. Dee, H. Dolman, M. Dowell, R. Engelen, K. Holmlund, G. Janssens-Maenhout, Y. Meijer, P. Palmer, M. Scholze, H. Denier van der Gon, M. Heimann, O. Juvyns, A. Kentarchos, and H. Zunker.
   An Operational Anthropogenic CO_2 Emissions Monitoring & Verification Support Capacity - Needs and high level requirements for in situ measurements.
   Technical Report EUR 29817 EN, European Commission Joint Research Centre, 2019.
3. Pinty B., G. Janssens-Maenhout, M. Dowell, H. Zunker, T. Brunhes, P. Ciais, D. Dee, H. Denier van der Gon, H. Dolman, M. Drinkwater, R. Engelen, M. Heimann, K. Holmlund, R. Husband, A. Kentarchos, Y. Meijer, P. Palmer, and M. Scholze.
   An Operational Anthropogenic CO_2 Emissions Monitoring & Verification Support capacity - Baseline Requirements, Model Components and Functional Architecture.
   Technical Report EUR 28736 EN, European Commission Joint Research Centre, 2017.
4. Peter Bergamaschi, Christian Frankenberg, Jan Fokke Meirink, Maarten Krol, M. Gabriella Villani, Sander Houweling, Frank Dentener, Edward J. Dlugokencky, John B. Miller, Luciana V. Gatti, Andreas Engel, and Ingeborg Levin.
   Inverse modeling of global and regional CH_4 emissions using SCIAMACHY satellite retrievals.
   Journal of Geophysical Research: Atmospheres, 114(D22), 2009.
5. Gurbir S. Bhullar, Peter J. Edwards, and Harry Olde Venterink.
   Variation in the plant-mediated methane transport and its importance for methane emission from intact wetland peat mesocosms.
   Journal of Plant Ecology, 6(4):298–304, 01 2013.
6. A. A. Bloom, K. W. Bowman, M. Lee, A. J. Turner, R. Schroeder, J. R. Worden, R. Weidner, K. C. McDonald, and D. J. Jacob.
   A global wetland methane emissions and uncertainty dataset for atmospheric chemical transport models (wetcharts version 1.0).
   Geoscientific Model Development, 10(6):2141–2156, 2017.
7. A. A. Bloom, T. Lauvaux, J. Worden, V. Yadav, R. Duren, S. P. Sander, and D. S. Schimel.
   What are the greenhouse gas observing system requirements for reducing fundamental biogeochemical process uncertainty? amazon wetland ch_4 emissions as a case study.
   Atmospheric Chemistry and Physics, 16(23):15199–15218, 2016.
8. H. Bovensmann, J. P. Burrows, M. Buchwitz, J. Frerick, S. NoÃČÂńl, V. V. Rozanov, K. V. Chance, and A. P. H. Goede.
   Sciamachy: Mission objectives and measurement modes.
   Journal of the Atmospheric Sciences, 56(2):127 – 150, 01 Jan. 1999.
9. R. Brownlow, D. Lowry, R. E. Fisher, J. L. France, M. Lanoisellé, B. White, M. J. Wooster, T. Zhang, and E. G. Nisbet.
   Isotopic ratios of tropical methane emissions by atmospheric measurement.
   Global Biogeochemical Cycles, 31(9):1408–1419, 2017.
10. M. Buchwitz, R. de Beek, J. P. Burrows, H. Bovensmann, T. Warneke, J. Notholt, J. F. Meirink, A. P. H. Goede, P. Bergamaschi, S. Körner, M. Heimann, and A. Schulz.
    Atmospheric methane and carbon dioxide from SCIAMACHY satellite data: initial comparison with chemistry and transport models.
    Atmospheric Chemistry and Physics, 5(4):941–962, 2005.
11. A. Butz, S. Guerlet, O. Hasekamp, D. Schepers, A. Galli, I. Aben, C. Frankenberg, J.-M. Hartmann, H. Tran, A. Kuze, G. Keppel-Aleks, G. Toon, D. Wunch, P. Wennberg, N. Deutscher, D. Griffith, R. Macatangay, J. Messerschmidt, J. Notholt, and T. Warneke.
    Toward accurate CO2and CH4observations from GOSAT.
    Geophysical Research Letters, 38(14), 2011.
12. S. Crowell, D. Baker, A. Schuh, S. Basu, A. R. Jacobson, F. Chevallier, J. Liu, F. Deng, L. Feng, K. McKain, A. Chatterjee, J. B. Miller, B. B. Stephens, A. Eldering, D. Crisp, D. Schimel, R. Nassar, C. W. O'Dell, T. Oda, C. Sweeney, P. I. Palmer, and D. B. A. Jones.

The 2015–2016 carbon cycle as seen from OCO-2 and the global in situ network.
Atmospheric Chemistry and Physics, 19(15):9797–9831, 2019.

13. Joost A. de Gouw, J. Pepijn Veefkind, Esther Roosenbrand, Barbara Dix, John C. Lin, Jochen Landgraf, and Pieternel F. Levelt.
Daily satellite observations of methane from oil and gas production regions in the United States.
Scientific Reports, 10(1), jan 2020.
14. E. Etiope.
Natural Gas Seepage: The Earth's Hydrocarbon Degassing.
Springer, 2015.
15. L. Feng, P. I. Palmer, H. Bösch, R. J. Parker, A. J. Webb, C. S. C. Correia, N. M. Deutscher, L. G. Domingues, D. G. Feist, L. V. Gatti, E. Gloor, F. Hase, R. Kivi, Y. Liu, J. B. Miller, I. Morino, R. Sussmann, K. Strong, O. Uchino, J. Wang, and A. Zahn.
Consistent regional fluxes of CH_4 and CO_2 inferred from GOSAT proxy $XCH_4 : XCO_2$ retrievals, 2010–2014.
Atmospheric Chemistry and Physics, 17(7):4781–4797, 2017.
16. C. Frankenberg, I. Aben, P. Bergamaschi, E. J. Dlugokencky, R. van Hees, S. Houweling, P. van der Meer, R. Snel, and P. Tol.
Global column-averaged methane mixing ratios from 2003 to 2009 as derived from SCIAMACHY: Trends and variability.
Journal of Geophysical Research: Atmospheres, 116(D4), 2011.
17. A. Fraser, P. I. Palmer, L. Feng, H. Boesch, A. Cogan, R. Parker, E. J. Dlugokencky, P. J. Fraser, P. B. Krummel, R. L. Langenfelds, S. O'Doherty, R. G. Prinn, L. P. Steele, M. van der Schoot, and R. F. Weiss.
Estimating regional methane surface fluxes: the relative importance of surface and GOSAT mole fraction measurements.
Atmospheric Chemistry and Physics, 13(11):5697–5713, 2013.
18. A. Fraser, P. I. Palmer, L. Feng, H. Bösch, R. Parker, E. J. Dlugokencky, P. B. Krummel, and R. L. Langenfelds.
Estimating regional fluxes of CO_2 and CH_4 using space-borne observations of XCH_4: XCO_2.
Atmospheric Chemistry and Physics, 14(23):12883–12895, 2014.
19. I. Fung, J. John, J. Lerner, E. Matthews, M. Prather, L. P. Steele, and P. J. Fraser.
Three-dimensional model synthesis of the global methane cycle.
Journal of Geophysical Research: Atmospheres, 96(D7):13033–13065, 1991.
20. Anita L. Ganesan, Matt Rigby, Mark F. Lunt, Robert J. Parker, Hartmut Boesch, N. Goulding, Taku Umezawa, Andreas Zahn, Abhijit Chatterjee, Ronald G. Prinn, Yogesh K. Tiwari, Marcel van der Schoot, and Paul B. Krummel.
Atmospheric observations show accurate reporting and little growth in Indian methane emissions.
Nature Communications, 8(1):836–837, 2017.
21. Australian Government.
National greenhouse gas and energy reporting: Safeguard facilities data.
Online, December 2020.
http://www.cleanenergyregulator.gov.au/NGER/.
22. Kevin Robert Gurney, Rachel M. Law, A. Scott Denning, Peter J. Rayner, David Baker, Philippe Bousquet, Lori Bruhwiler, Yu-Han Chen, Philippe Ciais, Songmiao Fan, Inez Y. Fung, Manuel Gloor, Martin Heimann, Kaz Higuchi, Jasmin John, Takashi Maki, Shamil Maksyutov, Ken Masarie, Philippe Peylin, Michael Prather, Bernard C. Pak, James Randerson, Jorge Sarmiento, Shoichi Taguchi, Taro Takahashi, and Chiu-Wai Yuen.
Towards robust regional estimates of CO_2 sources and sinks using atmospheric transport models.
Nature, 415(6872):626–630, 2002.
23. P. Hausmann, R. Sussmann, and D. Smale.
Contribution of oil and natural gas production to renewed increase in atmospheric methane (2007–2014): top–down estimate from ethane and methane column observations.
Atmospheric Chemistry and Physics, 16(5):3227–3244, 2016.
24. Haili Hu, Jochen Landgraf, Rob Detmers, Tobias Borsdorff, Joost Aan de Brugh, Ilse Aben, Andre Butz, and Otto Hasekamp.

Toward global mapping of methane with TROPOMI: First results and intersatellite comparison to GOSAT.
Geophysical Research Letters, 45(8):3682–3689, 2018.

25. D. J. Jacob, A. J. Turner, J. D. Maasakkers, J. Sheng, K. Sun, X. Liu, K. Chance, I. Aben, J. McKeever, and C. Frankenberg.
Satellite observations of atmospheric methane and their value for quantifying methane emissions.
Atmospheric Chemistry and Physics, 16(22):14371–14396, 2016.
26. G. Janssens-Maenhout, M. Crippa, D. Guizzardi, M. Muntean, E. Schaaf, F. Dentener, P. Bergamaschi, V. Pagliari, J. G. J. Olivier, J. A. H. W. Peters, J. A. van Aardenne, S. Monni, U. Doering, A. M. R. Petrescu, E. Solazzo, and G. D. Oreggioni.
EDGAR v4.3.2 global atlas of the three major greenhouse gas emissions for the period 1970–2012.
Earth System Science Data, 11(3):959–1002, 2019.
27. Akihiko Kuze, Hiroshi Suto, Masakatsu Nakajima, and Takashi Hamazaki.
Thermal and near infrared sensor for carbon observation Fourier-transform spectrometer on the Greenhouse Gases Observing Satellite for greenhouse gases monitoring.
Appl. Opt., 48(35):6716–6733, Dec 2009.
28. Keith A. Kvenvolden and Bruce W. Rogers.
Gaia's breath: global methane exhalations.
Marine and Petroleum Geology, 22(4):579–590, 2005.
Near-Surface Hydrocarbon Migration: Mechanisms and Seepage Rates.
29. Simon L. Lewis, Paulo M. Brando, Oliver L. Phillips, Geertje M. F. van der Heijden, and Daniel Nepstad.
The 2010 Amazon drought.
Science, 331(6017):554–554, 2011.
30. Junjie Liu, Kevin W. Bowman, David S. Schimel, Nicolas C. Parazoo, Zhe Jiang, Meemong Lee, A. Anthony Bloom, Debra Wunch, Christian Frankenberg, Ying Sun, Christopher W. O'Dell, Kevin R. Gurney, Dimitris Menemenlis, Michelle Gierach, David Crisp, and Annmarie Eldering.
Contrasting carbon cycle responses of the tropical continents to the 2015–2016 El Niño.
Science, 358(6360), 2017.
31. Alba Lorente, Tobias Borsdorff, Andre Butz, Otto Hasekamp, Joost aan de Brugh, Andreas Schneider, Lianghai Wu, Frank Hase, Rigel Kivi, Debra Wunch, David F. Pollard, Kei Shiomi, Nicholas M. Deutscher, Voltaire A. Velazco, Coleen M. Roehl, Paul O. Wennberg, Thorsten Warneke, and Jochen Landgraf.
Methane retrieved from TROPOMI: improvement of the data product and validation of the first 2 years of measurements.
Atmospheric Measurement Techniques, 14(1):665–684, jan 2021.
32. M. F. Lunt, P. I. Palmer, L. Feng, C. M. Taylor, H. Boesch, and R. J. Parker.
An increase in methane emissions from tropical Africa between 2010 and 2016 inferred from satellite data.
Atmospheric Chemistry and Physics, 19(23):14721–14740, 2019.
33. Mark F Lunt, Paul I Palmer, Alba Lorente, Tobias Borsdorff, Jochen Landgraf, Robert J Parker, and Hartmut Boesch.
Rain-fed pulses of methane from East Africa during 2018–2019 contributed to atmospheric growth rate.
Environmental Research Letters, 16(2):024021, feb 2021.
34. J. D. Maasakkers, D. J. Jacob, M. P. Sulprizio, T. R. Scarpelli, H. Nesser, J.-X. Sheng, Y. Zhang, M. Hersher, A. A. Bloom, K. W. Bowman, J. R. Worden, G. Janssens-Maenhout, and R. J. Parker.
Global distribution of methane emissions, emission trends, and oh concentrations and trends inferred from an inversion of gosat satellite data for 2010–2015.
Atmospheric Chemistry and Physics, 19(11):7859–7881, 2019.
35. Jingqiu Mao, Fabien Paulot, Daniel J. Jacob, Ronald C. Cohen, John D. Crounse, Paul O. Wennberg, Christoph A. Keller, Rynda C. Hudman, Michael P. Barkley, and Larry W. Horowitz.
Ozone and organic nitrates over the eastern United States: Sensitivity to isoprene chemistry.
Journal of Geophysical Research: Atmospheres, 118(19):11,256–11,268, 2013.

36. J. McNorton, C. Wilson, M. Gloor, R. J. Parker, H. Boesch, W. Feng, R. Hossaini, and M. P. Chipperfield.
Attribution of recent increases in atmospheric methane through 3-d inverse modelling.
Atmospheric Chemistry and Physics, 18(24):18149–18168, 2018.
37. Scot M. Miller, Anna M. Michalak, Robert G. Detmers, Otto P. Hasekamp, Lori M. P. Bruhwiler, and Stefan Schwietzke.
China's coal mine methane regulations have not curbed growing emissions.
Nature Communications, 10(1):303–304, 2019.
38. G. Myhre, D. Shindell, F.-M. Bréon, W. Collins, J. Fuglestvedt, J. Huang, D. Koch, J.-F. Lamarque, D. Lee, B. Mendoza, T. Nakajima, A. Robock, G. Stephens, T. Takemura, and H. Zhang.
Climate Change 2013: The Physical Science Basis. Contribution of Working Group I to the Fifth Assessment Report of the Intergovernmental Panel on Climate Change, chapter Anthropogenic and Natural Radiative Forcing.
Cambridge University Press, United Kingdom and New York, NY, USA, 2013.
39. E. G. Nisbet, E. J. Dlugokencky, M. R. Manning, D. Lowry, R. E. Fisher, J. L. France, S. E. Michel, J. B. Miller, J. W. C. White, B. Vaughn, P. Bousquet, J. A. Pyle, N. J. Warwick, M. Cain, R. Brownlow, G. Zazzeri, M. LanoisellÃČÂl', A. C. Manning, E. Gloor, D. E. J. Worthy, E.-G. Brunke, C. Labuschagne, E. W. Wolff, and A. L. Ganesan.
Rising atmospheric methane: 2007–2014 growth and isotopic shift.
Global Biogeochemical Cycles, 30(9):1356–1370, 2016.
40. E. G. Nisbet, M. R. Manning, E. J. Dlugokencky, R. E. Fisher, D. Lowry, S. E. Michel, C. Lund Myhre, S. M. Platt, G. Allen, P. Bousquet, R. Brownlow, M. Cain, J. L. France, O. Hermansen, R. Hossaini, A. E. Jones, I. Levin, A. C. Manning, G. Myhre, J. A. Pyle, B. H. Vaughn, N. J. Warwick, and J. W. C. White.
Very Strong Atmospheric Methane Growth in the 4 Years 2014-2017: Implications for the Paris Agreement.
Global Biogeochemical Cycles, 33(3):318–342, 2019.
41. Ilissa B Ocko, Tianyi Sun, Drew Shindell, Michael Oppenheimer, Alexander N Hristov, Stephen W Pacala, Denise L Mauzerall, Yangyang Xu, and Steven P Hamburg.
Acting rapidly to deploy readily available methane mitigation measures by sector can immediately slow global warming.
Environmental Research Letters, 16(5):054042, may 2021.
42. T. Oda and S. Maksyutov.
A very high-resolution (1 km x 1 km) global fossil fuel CO_2 emission inventory derived using a point source database and satellite observations of nighttime lights.
Atmospheric Chemistry and Physics, 11(2):543–556, 2011.
43. C. W. O'Dell, A. Eldering, P. O. Wennberg, D. Crisp, M. R. Gunson, B. Fisher, C. Frankenberg, M. Kiel, H. Lindqvist, L. Mandrake, A. Merrelli, V. Natraj, R. R. Nelson, G. B. Osterman, V. H. Payne, T. E. Taylor, D. Wunch, B. J. Drouin, F. Oyafuso, A. Chang, J. McDuffie, M. Smyth, D. F. Baker, S. Basu, F. Chevallier, S. M. R. Crowell, L. Feng, P. I. Palmer, M. Dubey, O. E. García, D. W. T. Griffith, F. Hase, L. T. Iraci, R. Kivi, I. Morino, J. Notholt, H. Ohyama, C. Petri, C. M. Roehl, M. K. Sha, K. Strong, R. Sussmann, Y. Te, O. Uchino, and V. A. Velazco.
Improved retrievals of carbon dioxide from Orbiting Carbon Observatory-2 with the version 8 ACOS algorithm.
Atmospheric Measurement Techniques, 11(12):6539–6576, 2018.
44. S. C. Olsen and J. T. Randerson.
Differenecs between surface and column atmospheric CO_2 and implications for carbon cycle research.
J. Geophys. Res., 2004.
45. P. I. Palmer.
The role of satellite observations in understanding the impact of El Niño on the carbon cycle: current capabilities and future opportunities.
Phil. Trans. R. Soc. B, 373, 2018.
46. Paul I. Palmer, Liang Feng, David Baker, Frédéric Chevallier, Hartmut Bösch, and Peter Somkuti.
Net carbon emissions from african biosphere dominate pan-tropical atmospheric CO_2 signal.
Nature Communications, 10(1):3344, 2019.

47. S. Pandey, S. Houweling, M. Krol, I. Aben, F. Chevallier, E. J. Dlugokencky, L. V. Gatti, E. Gloor, J. B. Miller, R. Detmers, T. Machida, and T. Röckmann.
Inverse modeling of GOSAT-retrieved ratios of total column CH_4 and CO_2 for 2009 and 2010.
Atmospheric Chemistry and Physics, 16(8):5043–5062, 2016.
48. Sudhanshu Pandey, Ritesh Gautam, Sander Houweling, Hugo Denier van der Gon, Pankaj Sadavarte, Tobias Borsdorff, Otto Hasekamp, Jochen Landgraf, Paul Tol, Tim van Kempen, Ruud Hoogeveen, Richard van Hees, Steven P. Hamburg, Joannes D. Maasakkers, and Ilse Aben.
Satellite observations reveal extreme methane leakage from a natural gas well blowout.
Proceedings of the National Academy of Sciences, 116(52):26376–26381, dec 2019.
49. R. Parker and H. Boesch.
University of leicester GOSAT proxy XCH4 v9.0.
Centre for Environmental Data Analysis, 7 May 2020.
50. R. J. Parker, H. Boesch, K. Byckling, A. J. Webb, P. I. Palmer, L. Feng, P. Bergamaschi, F. Chevallier, J. Notholt, N. Deutscher, T. Warneke, F. Hase, R. Sussmann, S. Kawakami, R. Kivi, D. W. T. Griffith, and V. Velazco.
Assessing 5 years of GOSAT Proxy XCH_4 data and associated uncertainties.
Atmospheric Measurement Techniques, 8(11):4785–4801, 2015.
51. R. J. Parker, A. Webb, H. Boesch, P. Somkuti, R. Barrio Guillo, A. Di Noia, N. Kalaitzi, J. Anand, P. Bergamaschi, F. Chevallier, P. I. Palmer, L. Feng, N. M. Deutscher, D. G. Feist, D. W. T. Griffith, F. Hase, R. Kivi, I. Morino, J. Notholt, Y.-S. Oh, H. Ohyama, C. Petri, D. F. Pollard, C. Roehl, M. K. Sha, K. Shiomi, K. Strong, R. Sussmann, Y. Te, V. A. Velazco, T. Warneke, P. O. Wennberg, and D. Wunch.
A Decade of GOSAT Proxy Satellite CH_4 Observations.
Earth System Science Data Discussions, 2020:1–36, 2020.
52. Robert Parker, Hartmut Boesch, Austin Cogan, Annemarie Fraser, Liang Feng, Paul I. Palmer, Janina Messerschmidt, Nicholas Deutscher, David W. T. Griffith, Justus Notholt, Paul O. Wennberg, and Debra Wunch.
Methane observations from the Greenhouse Gases Observing SATellite: Comparison to ground-based TCCON data and model calculations.
Geophysical Research Letters, 38(15), 2011.
53. Robert J. Parker, Hartmut Boesch, Joe McNorton, Edward Comyn-Platt, Manuel Gloor, Chris Wilson, Martyn P. Chipperfield, Garry D. Hayman, and A. Anthony Bloom.
Evaluating year-to-year anomalies in tropical wetland methane emissions using satellite ch4 observations.
Remote Sensing of Environment, 211:261–275, 2018.
54. P. K. Patra, S. Houweling, M. Krol, P. Bousquet, D. Belikov, D. Bergmann, H. Bian, P. Cameron-Smith, M. P. Chipperfield, K. Corbin, A. Fortems-Cheiney, A. Fraser, E. Gloor, P. Hess, A. Ito, S. R. Kawa, R. M. Law, Z. Loh, S. Maksyutov, L. Meng, P. I. Palmer, R. G. Prinn, M. Rigby, R. Saito, and C. Wilson.
TransCom model simulations of CH_4 and related species: linking transport, surface flux and chemical loss with CH_4 variability in the troposphere and lower stratosphere.
Atmospheric Chemistry and Physics, 11(24):12813–12837, 2011.
55. Michael J. Prather, Christopher D. Holmes, and Juno Hsu.
Reactive greenhouse gas scenarios: Systematic exploration of uncertainties and the role of atmospheric chemistry.
Geophysical Research Letters, 39(9), 2012.
56. Andrew L. Rice, Christopher L. Butenhoff, Doaa G. Teama, Florian H. Röger, M. Aslam K. Khalil, and Reinhold A. Rasmussen.
Atmospheric methane isotopic record favors fossil sources flat in 1980s and 1990s with recent increase.
Proceedings of the National Academy of Sciences, 113(39):10791–10796, 2016.
57. M. Rigby, R. G. Prinn, P. J. Fraser, P. G. Simmonds, R. L. Langenfelds, J. Huang, D. M. Cunnold, L. P. Steele, P. B. Krummel, R. F. Weiss, S. O'Doherty, P. K. Salameh, H. J. Wang, C. M. Harth, J. MÃČÅŠhle, and L. W. Porter.
Renewed growth of atmospheric methane.
Geophysical Research Letters, 35(22), 2008.
58. Matthew Rigby, Stephen A. Montzka, Ronald G. Prinn, James W. C. White, Dickon Young,

Simon O'Doherty, Mark F. Lunt, Anita L. Ganesan, Alistair J. Manning, Peter G. Simmonds, Peter K. Salameh, Christina M. Harth, Jens Mühle, Ray F. Weiss, Paul J. Fraser, L. Paul Steele, Paul B. Krummel, Archie McCulloch, and Sunyoung Park.
Role of atmospheric oxidation in recent methane growth.
Proceedings of the National Academy of Sciences, 114(21):5373–5377, 2017.

59. M. Saunois, A. R. Stavert, B. Poulter, P. Bousquet, J. G. Canadell, R. B. Jackson, P. A. Raymond, E. J. Dlugokencky, S. Houweling, P. K. Patra, P. Ciais, V. K. Arora, D. Bastviken, P. Bergamaschi, D. R. Blake, G. Brailsford, L. Bruhwiler, K. M. Carlson, M. Carrol, S. Castaldi, N. Chandra, C. Crevoisier, P. M. Crill, K. Covey, C. L. Curry, G. Etiope, C. Frankenberg, N. Gedney, M. I. Hegglin, L. Höglund-Isaksson, G. Hugelius, M. Ishizawa, A. Ito, G. Janssens-Maenhout, K. M. Jensen, F. Joos, T. Kleinen, P. B. Krummel, R. L. Langenfelds, G. G. Laruelle, L. Liu, T. Machida, S. Maksyutov, K. C. McDonald, J. McNorton, P. A. Miller, J. R. Melton, I. Morino, J. Müller, F. Murguia-Flores, V. Naik, Y. Niwa, S. Noce, S. O'Doherty, R. J. Parker, C. Peng, S. Peng, G. P. Peters, C. Prigent, R. Prinn, M. Ramonet, P. Regnier, W. J. Riley, J. A. Rosentreter, A. Segers, I. J. Simpson, H. Shi, S. J. Smith, L. P. Steele, B. F. Thornton, H. Tian, Y. Tohjima, F. N. Tubiello, A. Tsuruta, N. Viovy, A. Voulgarakis, T. S. Weber, M. van Weele, G. R. van der Werf, R. F. Weiss, D. Worthy, D. Wunch, Y. Yin, Y. Yoshida, W. Zhang, Z. Zhang, Y. Zhao, B. Zheng, Q. Zhu, Q. Zhu, and Q. Zhuang.
The global methane budget 2000–2017.
Earth System Science Data, 12(3):1561–1623, 2020.
60. Hinrich Schaefer, Sara E. Mikaloff Fletcher, Cordelia Veidt, Keith R. Lassey, Gordon W. Brailsford, Tony M. Bromley, Edward J. Dlugokencky, Sylvia E. Michel, John B. Miller, Ingeborg Levin, Dave C. Lowe, Ross J. Martin, Bruce H. Vaughn, and James W. C. White.
A 21st-century shift from fossil-fuel to biogenic methane emissions indicated by $13CH_4$.
Science, 352(6281):80–84, 2016.
61. Stefan Schwietzke, Owen A. Sherwood, Lori M. P. Bruhwiler, John B. Miller, Giuseppe Etiope, Edward J. Dlugokencky, Sylvia Englund Michel, Victoria A. Arling, Bruce H. Vaughn, James W. C. White, and Pieter P. Tans.
Upward revision of global fossil fuel methane emissions based on isotope database.
Nature, 538(7623):88–91, 2016.
62. O. A. Sherwood, S. Schwietzke, V. A. Arling, and G. Etiope.
Global inventory of gas geochemistry data from fossil fuel, microbial and burning sources, version 2017.
Earth System Science Data, 9(2):639–656, 2017.
63. A. F. Siegel.
Robust regression using repeated medians.
Technical report, Princeton University, 1980.
64. L. Surl, P. I. Palmer, and G. González Abad.
Which processes drive observed variations of HCHO columns over India?
Atmospheric Chemistry and Physics, 18(7):4549–4566, 2018.
65. Taro Takahashi, Stewart C. Sutherland, Rik Wanninkhof, Colm Sweeney, Richard A. Feely, David W. Chipman, Burke Hales, Gernot Friederich, Francisco Chavez, Christopher Sabine, Andrew Watson, Dorothee C.E. Bakker, Ute Schuster, Nicolas Metzl, Hisayuki Yoshikawa-Inoue, Masao Ishii, Takashi Midorikawa, Yukihiro Nojiri, Arne KÃČÂűrtzinger, Tobias Steinhoff, Mario Hoppema, Jon Olafsson, Thorarinn S. Arnarson, Bronte Tilbrook, Truls Johannessen, Are Olsen, Richard Bellerby, C.S. Wong, Bruno Delille, N.R. Bates, and Hein J.W. de Baar.
Climatological mean and decadal change in surface ocean pco2, and net seaÃćÂĂÂŞair co2 flux over the global oceans.
Deep Sea Research Part II: Topical Studies in Oceanography, 56(8):554–577, 2009.
Surface Ocean CO2 Variability and Vulnerabilities.
66. R. L. Thompson, E. G. Nisbet, I. Pisso, A. Stohl, D. Blake, E. J. Dlugokencky, D. Helmig, and J. W. C. White.
Variability in atmospheric methane from fossil fuel and microbial sources over the last three decades.
Geophysical Research Letters, 45(20):11,499–11,508, 2018.
67. A. J. Turner, D. J. Jacob, K. J. Wecht, J. D. Maasakkers, E. Lundgren, A. E. Andrews, S. C. Biraud, H. Boesch, K. W. Bowman, N. M. Deutscher, M. K. Dubey, D. W. T. Griffith, F. Hase,

A. Kuze, J. Notholt, H. Ohyama, R. Parker, V. H. Payne, R. Sussmann, C. Sweeney, V. A. Velazco, T. Warneke, P. O. Wennberg, and D. Wunch.
Estimating global and North American methane emissions with high spatial resolution using GOSAT satellite data.
Atmospheric Chemistry and Physics, 15(12):7049–7069, 2015.

68. Alexander J. Turner, Christian Frankenberg, Paul O. Wennberg, and Daniel J. Jacob.
Ambiguity in the causes for decadal trends in atmospheric methane and hydroxyl.
Proceedings of the National Academy of Sciences, 114(21):5367–5372, 2017.
69. G. R. van der Werf, J. T. Randerson, L. Giglio, G. J. Collatz, M. Mu, P. S. Kasibhatla, D. C. Morton, R. S. DeFries, Y. Jin, and T. T. van Leeuwen.
Global fire emissions and the contribution of deforestation, savanna, forest, agricultural, and peat fires (1997-2009).
Atmospheric Chemistry and Physics, 10(23):11707–11735, 2010.
70. D. J. Varon, J. McKeever, D. Jervis, J. D. Maasakkers, S. Pandey, S. Houweling, I. Aben, T. Scarpelli, and D. J. Jacob.
Satellite discovery of anomalously large methane point sources from oil/gas production.
Geophysical Research Letters, 46(22):13507–13516, nov 2019.
71. Alex J. Webb, Hartmut BÃČÂűsch, Robert J. Parker, Luciana V. Gatti, Emanuel Gloor, Paul I. Palmer, Luana S. Basso, Martyn P. Chipperfield, Caio S. C. Correia, Lucas G. Domingues, Liang Feng, Siegfried Gonzi, John B. Miller, Thorsten Warneke, and Christopher Wilson.
CH_4 concentrations over the Amazon from GOSAT consistent with in situ vertical profile data.
Journal of Geophysical Research: Atmospheres, 121(18):11,006–11,020, 2016.
72. C. Wilson, M. P. Chipperfield, M. Gloor, R. J. Parker, H. Boesch, J. McNorton, L. V. Gatti, J. B. Miller, L. S. Basso, and S. A. Monks.
Large and increasing methane emissions from eastern amazonia derived from satellite data, 2010–2018.
Atmospheric Chemistry and Physics Discussions, 2020:1–38, 2020.
73. C. Wilson, M. P. Chipperfield, M. Gloor, R. J. Parker, H. Boesch, J. McNorton, L. V. Gatti, J. B. Miller, L. S. Basso, and S. A. Monks.
Large and increasing methane emissions from Eastern Amazonia derived from satellite data, 2010–2018.
Atmospheric Chemistry and Physics Discussions, 2020:1–38, 2020.
74. John R. Worden, A. Anthony Bloom, Sudhanshu Pandey, Zhe Jiang, Helen M. Worden, Thomas W. Walker, Sander Houweling, and Thomas Röckmann.
Reduced biomass burning emissions reconcile conflicting estimates of the post-2006 atmospheric methane budget.
Nature Communications, 8(1):2227, 2017.
75. Debra Wunch, Geoffrey C. Toon, Jean-Francois L. Blavier, Rebecca A. Washenfelder, Justus Notholt, Brian J. Connor, David W. T. Griffith, Vanessa Sherlock, and Paul O. Wennberg.
The Total Carbon Column Observing Network.
Philosophical Transactions of the Royal Society A: Mathematical, Physical and Engineering Sciences, 369(1943):2087–2112, 2011.
76. G. Zazzeri, D. Lowry, R. E. Fisher, J. L. France, M. Lanoisellé, C. S. B. Grimmond, and E. G. Nisbet.
Evaluating methane inventories by isotopic analysis in the London region.
Scientific Reports, 7(1):4854, 2017.
77. Yuzhong Zhang, Ritesh Gautam, Sudhanshu Pandey, Mark Omara, Joannes D. Maasakkers, Pankaj Sadavarte, David Lyon, Hannah Nesser, Melissa P. Sulprizio, Daniel J. Varon, Ruixiong Zhang, Sander Houweling, Daniel Zavala-Araiza, Ramon A. Alvarez, Alba Lorente, Steven P. Hamburg, Ilse Aben, and Daniel J. Jacob.
Quantifying methane emissions from the largest oil-producing basin in the United States from space.
Science Advances, 6(17):eaaz5120, apr 2020.
78. Zhen Zhang, Niklaus E Zimmermann, Leonardo Calle, George Hurtt, Abhishek Chatterjee, and Benjamin Poulter.
Enhanced response of global wetland methane emissions to the 2015–2016 El Niño-Southern Oscillation event.

Environmental Research Letters, 13(7):074009, 2018.

79. Lei Zhu, Daniel J Jacob, Loretta J Mickley, Eloise A Marais, Daniel S Cohan, Yasuko Yoshida, Bryan N Duncan, Gonzalo Gonzalez Abad, and Kelly V Chance.
Anthropogenic emissions of highly reactive volatile organic compounds in eastern Texas inferred from oversampling of satellite (OMI) measurements of HCHO columns.
Environmental Research Letters, 9(11):114004, nov 2014.